Grant agreement no. 668294
PHC-14-2015 'New therapies for rare diseases'

- Research and Innovation Action -

D5.1 - Analysis of TEI in mouse

WP 5 - Transplantation of engineered intestine

Due date of deliverable: month 45

Actual submission date: 1612/2019

Start date of project: 01/01/2016 Duration: 60 months

Lead beneficiary for this deliverable: CHLA

Last editor: Tracy Grikscheit

Contributors: Tracy Grikscheit, Vivian Li, Paolo De Coppi

Dissemination Level		
PU	Public	X
PP	Restricted to other programme participants (including the Commission Services)	
RE	Restricted to a group specified by the consortium (including the Commission Services)	
CO	Confidential, only for members of the consortium (including the Commission Services)	

History table

Version	Date	Released by	Comments
1.0	30.10.2019	Tracy Grikscheit	n.a.

Table of contents

1. Introduction

Intestinal failure (IF), following extensive anatomical or functional loss of small intestine (SI), has debilitating long-term effects on infants and children with this condition. Priority of care is to increase the child's length of functional intestine, jejunum in particular, to improve nutritional independence. Here we report a robust protocol for reconstruction of autologous intestinal mucosal grafts using primary IF patient materials. Human jejunal intestinal organoids derived from pediatric IF patients can be expanded efficiently *in vitro* with region-specific markers preserved after long term culture. Decellularized human intestinal matrix with intact ultrastructure is used as biological scaffolds. Proteomic and Raman spectroscopic analyses reveal highly analogous biochemical composition of decellularized human SI and colon matrix, implying that they can both be utilized as scaffolds for jejunal graft reconstruction. Indeed, seeding of primary human jejunal organoids to either SI or colonic scaffolds *in vitro* can efficiently reconstruct functional jejunal grafts with persistent disaccharidase activity as early as 4 days after seeding, which can further survive and mature after transplantation *in vivo*. Our findings pave the way towards regenerative medicine for IF patients.

1.1 General context

Infants with intestinal failure (IF) have a reduction in functional intestinal mass below the minimal requirement to satisfy nutrient and fluid needs to sustain growth. This may be caused by anatomical loss due to short bowel syndrome (SBS), dysmaturity due to neuromuscular intestinal diseases, or congenital epithelial defects of the intestine[2]. IF patients may become dependent on
intravenous feeding known as parenteral nutrition (PN), which is associated with numerous complications including bacterial overgrowth, line sepsis, central venous access thrombosis or PN related liver disease[3,4]. Ultimately, children with irreversible IF are referred for small bowel transplantation. However, many children die on the transplant waiting list due to shortage of suitable organs. Among those who receive a transplant, patient survival at 5 years is only 58% due to sepsis, graft failure and complications of long-term immunosuppression[5]. Given the high morbidity and mortality associated with current treatment for IF, there is an urgent unmet clinical need for research into novel treatment strategies for these patients. Autologous tissue engineering of functional intestinal grafts, through combination of biomaterials and patient-derived cells, presents an innovative alternative approach to treat IF patients[6]. Multiple studies have previously reported the pre-clinical developments of tissue engineering methodologies in other organs such as esophageal, skeletal muscle, liver and lung reconstruction. However, while engineering of simpler tissues such as skin and cornea are established in clinical practice examples of successful clinical applications of more complex organs have only been demonstrated in few case reports of airway and bladder reconstruction. To date there have been no clinical studies of bioengineered small intestinal grafts in humans. Intestinal reconstruction using patient-derived cells would negate the need for immunosuppression, which would circumvent the complications of graft-host rejection, and risk of infection and cancer[5]. Furthermore, tissue engineering strategies to IF should enable personalized grafts whereby length, and cellular or scaffold composition may be modified based on the individual patient's condition. For instance, SBS is a consequence of massive full thickness anatomical 60 loss of the small intestine, leading to inadequate enteral absorption. The most predominant pathologies of pediatric SBS include necrotizing enterocolitis, intestinal atresia, gastroschisis, malrotation with volvulus and Crohn's disease[4], which require reconstruction of a full thickness intestinal wall graft (including mucosa, submucosa and muscularis layers) to fit infant's dimensions. On the other hand, patients with neuromuscular intestinal diseases such as extensive Hirschsprung's disease usually have a healthy intestinal epithelium but dysfunctional neuromuscular wall, where reconstruction of a neuromuscular graft capable of peristalsis is paramount[21]. Conversely, patients with

congenital epithelial defects such as Microvillus Inclusion Disease retain intact neuromuscular function[22]. Thus, reconstruction of a purely mucosal graft with gene correction would be most beneficial to these patients. The success of tissue engineering requires optimal source of cells and scaffolds[23]. Intestinal cells could be derived from human induced pluripotent stem cells (hiPSCs), human embryonic stem cells (hESCs) or primary human somatic intestinal stem cells (hISCs). To achieve autologous transplantation, patient-derived hiPSCs and hISCs are the preferred options. While iPSCs have high potential to regenerate all the required cell sources needed for full thickness intestinal reconstruction, clinical use on paediatric patients remains controversial due to the potential risk of chromosomal aberrations and teratoma development during the reprogramming process. Recent advances on the establishment of 3-dimensional human intestinal organoid (hIO) culture system has revolutionised the field of regenerative medicine. These mini-hIO culture enables unlimited expansion of primary hISCs while maintaining multipotency and genetic stability. They are seemingly safer and ethically acceptable alternative cell source than hiPSCs for clinical use. However, the efficiency of establishing primary human small intestinal organoids derived from IF patients with limited starting materials has never been demonstrated. hISCs could be delivered using biodegradable materials such as polyglycolic 84 acid/poly-L-lactic acid polymers[31-33], however the lack of fine microarchitectural details as well as biological cues responsible for cell engraftment and self-organisation have so far largely limited their translation. On the other hand, biological extracellular matrix (ECM) obtained from decellularization of native organs represent a more physiological alternative to synthetic scaffolds.

1.2 Deliverable objectives

Here, we report a robust protocol to generate and expand hIOs derived from biopsies of pediatric IF patients undergoing endoscopy. We further optimize the decellularization protocol to native human intestinal tissues obtained from pediatric patients undergoing intestinal resections and perform in-depth characterization of the scaffold structure and composition. We focus on reconstruction of a functional jejunal graft, where majority of food digestion and absorption occurs and is crucial to restore nutritional autonomy in IF patients. Our results show that the engineered jejunal grafts can differentiate *in vitro* with digestion and absorption functions, which can further survive and form intestinal lumens *in vivo*. The current findings provide proof-of-concept to engineer autologous, functional and transplantable jejunal mucosal grafts derived from IF patients, and pave the way towards the ultimate reconstruction of full thickness intestinal graft for children with IF and SBS.

2. Methodological approach

METHODS

Animals and human tissue

Immune deficient NOD-SCID IL-2Rγnull (NSG) female mice, aged 9 - 14 weeks old, were used in all experiments (obtained from the Francis Crick Institute Biomedical Research Facility). All mice were housed in the animal facility at the Francis Crick Institute. All experiments were performed with ethical approval under Home Office Project License PPLs 70/8904 and 70/8560.

Porcine (Sus scrofa domesticus) SI from the 'Pietrain' breed was used to derive piglet SI scaffolds.

Piglets up to 3 kg in weight were euthanized following criteria outlined by the JSR veterinary advisors. Once sacrificed, the animals were transported to the lab via courier and the intestine was harvested immediately on arrival (within 6 hours of euthanasia).

Ethical approval for the use of human intestinal tissue was obtained from the Bloomsbury NRES Committee (REC reference 04-Q0508-79). The Committee was constituted in accordance with the Governance Arrangements for Research Ethics Committees and complied fully with the Standard Operating Procedures for Research Ethics Committees in the UK. Informed consent for the collection and use of human tissue was obtained from all

patients, parents or legal guardians at Great Ormond Street Hospital, London. Endoscopic biopsies for organoid isolation were sought from patients with an established diagnosis of intestinal failure on parenteral nutrition.
Surgical resections for scaffold fabrication were sought from patients undergoing stoma formation or closure procedures.

Organoid and fibroblast culture conditions
Endoscopic biopsy specimens were cut into finer pieces and washed in cold PBS. For organoid
isolation, the tissue fragments were incubated in 2mmol/L EDTA cold chelation buffer, consisting of distilled water with 5.6mmol/L Na2HPO4, 8mmol/L KH2PO4, 96.2mmol/L NaCl, 1.6mmol/L KCl, 43.4 mmol/L sucrose, 54.9 mmol/L D-sorbitol, 0.5mmol/L DL-dithiothreitol) for 30 minutes at 4°C as
previously reported[29]. Following this incubation period, crypts were released from the fragments by 21 shaking vigorously. The supernatant was centrifuged 466 at 800RPM for 5 minutes at 4°C, to form a pellet of intestinal crypts, which were washed in Advanced Dulbecco's modified Eagle medium (DMEM) / F12 supplemented with 5% penicillin/streptomycin, 10mmol/L HEPES and 2mM of GlutaMAX. The crypts were then resuspended in Basement Membrane Extract® (BME) and seeded in a single droplet on pre-heated 48-well plates. The BME was polymerised for 20 minutes at 37°C, before adding 250µL/well of either human IntestiCult™ Organoid Growth Medium (STEMCELL Technology, #06010) or human organoid basal culture media consisting of conditioned media produced using stably transfected L cells (Wnt 50%; R-spondin 10%; Noggin 5%) and the following growth factors: B12 1X (Invitrogen), Nicotinamide 10mM (Sigma-Aldrich), N-acetyl cysteine 1mM (Sigma-Aldrich), TGF-β type I receptor inhibitor A83-01 500nM (Tocris), P38 inhibitor SB202190 10µM(Sigma-Aldrich), Gastrin I 10nM (Sigma-Aldrich), EGF 50ng/ml (Invitrogen). Rho-kinase inhibitor Y-27632, 10µM was added to the culture media for the first week in culture, at a concentration of 10µM. The media of each well was changed every 2 days. Organoids in expansion were cultured in 3µM CHIR99021. Organoids in differentiation phase were cultured in 10µM DAPT for 48 hours. For the isolation of human intestinal fibroblasts, intestinal fragments left over from the chelation step above were washed in PBS and placed on the bottom of tissue culture dishes with DMEM supplemented with 10% heat inactivated Fetal Bovine Serum (FBS), antibiotics and 1% non-essential amino acids (all from Sigma-Aldrich). Fibroblasts grew from the fragments within 3-4 days. Cells used for seeding experiments were between passages 3-10.

3. Summary of activities and research findings

Robust generation and expansion of human small intestinal organoids derived from pediatric IF patients
The primary challenge of engineering autologous grafts for IF patients is to efficiently isolate and expand patient-derived intestinal epithelial cells from very limited starting materials such as endoscopic biopsies. To optimize the protocol, a maximum of two endoscopic intestinal epithelial biopsies (~2mm size) from pediatric patients were used for crypt isolation and organoid generation (Fig. 1a). In total, organoids were established from 11 individuals, among which 5 were diagnosed with IF clinically (Supplementary Table 1). On average, we were able to establish 3 to 5 organoid units from two endoscopic biopsies by week 4, which can be further expanded to over a million cells by week 8 for scaffold seeding (Fig. 1a-b). The expansion efficiency was similar in all three regions (duodenum, jejunum or ileum) of the small intestine (Fig. 1c). Quantitative reverse transcription-PCR (qRT-PCR) showed that the organoids expressed region-specific functional markers: the apical brush border enzyme cytochrome b reductase 1 (*CYBRD1*) and the iron transporter solute carrier family 40 member 1 (*SLC40A1*) in duodenal organoids; the brush border digestive enzymes sucrase isomaltase (*SI*) and lactase (*LCT*) in jejunal organoids; and the apical bile acid transporter (*SLC10A2*) and the basolateral organic solute transporter

(*OSTB*) in ileal organoids (Fig. 1d). We focused on the expansion and maintenance of jejunal organoids for subsequent graft reconstruction experiments as 90% of digestion and absorption of significant macro- and micro-nutrients occur in the proximal 100- 150cm of the jejunum[36]. Long-term culture of the jejunal organoids after significant passaging time (P > 25) were able to retain the expression of the region-specific functional markers, indicating that the organoids have cell intrinsic programme to retain their regional identities after prolonged culture (Fig. 1e).
Next, we tested the proliferation and differentiation potential of these jejunal organoids after prolonged expansion culture. In addition to the previously published human intestinal organoid media[29], we further treated the organoids with GSK3β 126 inhibitor (CHIR99021) to boost Wnt signaling and promote proliferation, or with gamma-secretase inhibitor (DAPT) to inhibit Notch signaling and drive differentiation. qRT-PCR analysis showed that stem cell (*OLFM4* and *LGR5*) and Paneth cell (*LYZ*) genes were significantly upregulated while differentiation genes (*MUC2*, *ALPI* and *CHGA*) were downregulated upon CHIR-treatment (Fig. 1f). A strong induction of proliferation was also observed in CHIR-treated organoids, which was accompanied by protein expression of proliferation (Ki67), stem cell (LGR5, SOX9) and Paneth cell (LYZ) markers (Fig. 1g-h). Conversely, DAPT-treated organoids displayed loss of stem cell and Paneth cell markers and gain of differentiation markers in both mRNA and protein levels (Fig. 1f, i), indicating that the differentiation capacity of these organoids was not affected by the prolonged expansion. Together, the results demonstrate that IF patient-derived organoids can be generated robustly from as little as two 2mm-biopsies, they multiply rapidly *ex vivo* under expansion media (+CHIR) while maintaining their initial regional identity and differentiation potential upon Notch inhibition (+DAPT).

Decellularization of human small intestinal and colonic ECM scaffolds
Previous studies have described decellularization protocols to generate rodent or piglet small intestinal (SI) ECM scaffolds. A more recent study has further attempted to fabricate human SI ECM scaffolds but failed to demonstrate successful decellularization[38]. Here we optimize the decellularization protocols for both human SI and colonic ECM scaffolds and compare their structural and biochemical compositions. Native human SI and colonic tissue was collected from pediatric patients undergoing intestinal resection (Supplementary Table 1), where circumferential intestinal adipose tissue was first dissected and removed from the serosal layer. Excess clinical intestinal tissues are often collected without intact mesentery, thus cannot be decellularized via perfusion. Instead, the native tissues were decellularized using detergent-enzymatic treatment (DET) via a series of immersion and agitation to remove all cellular components while preserving the microarchitecture. Indeed, histology analysis demonstrated absence of cellular and nuclei contents as revealed by H&E and DAPI staining in the decellularized scaffolds, w 151 hile the intestinal crypt-villus axis were well preserved (Fig. 2a,b). Immunofluorescent staining confirmed the presence of the key ECM protein collagen in both SI and colonic decellularized scaffolds
(Fig. 2a). The ultrastructure of the ECM scaffolds was further examined using scanning electron microscopy, which showed remarkable preservation of the microarchitecture of mucosa, submucosa and muscularis layers. Importantly, intact crypt-villus axis of the SI scaffold and crypts of the colonic scaffold in the mucosal layer was clearly identified after decellularization (Fig. 2c), which offer ideal natural biological platforms for organ reconstruction. In addition, we have also optimized the decellularization protocol of piglet SI confirming the removal of the nuclei and the remnants of the ECM component (Supplementary Fig. 1a,b) In particular, the decellularised tissue did not differ substantially from the fresh intestine in protein content, Collagen I, Collagen IV, Fibronectin, Laminin and macro-structure 162 (Supplementary Fig. 1c,d).

Compositional analyses of human small intestine and colon scaffolds
Next, we examined if the biomolecular composition of the scaffolds is also preserved after decellularization. Raman spectroscopy was used to compare the spectra profiles of the native tissues and their corresponding decellularized scaffolds. The overall spectra profiles

between native and decellularized scaffolds were highly analogous, indicating that the gross biomolecular composition was preserved (Fig. 3a). On the other hand, a handful of differential spectra was noted across the three tissue layers (mucosa, submucosa and muscle). For instance, the distinct nucleic acid peaks at 726cm^{-1}, 780cm^{-1} and 1575cm-1 wavenumber - indicative of the ring breathing mode of nucleotides - were detected preferentially in the native SI and colonic mucosa with dense cellular populations, where the peaks were either significantly reduced or absent in the decellularized scaffolds. Consistently, characteristic lipid peaks at 1078cm-1 and 1303cm^{-1} - indicative of the □(C-C) skeletal of acyl backbone of lipids and methylene bending mode - was also noted to be more intense in both native mucosa and muscle spectra, which could be associated with the lipid-rich cellular membranes of these two cell-enriched layers. Conversely, the spectral peak at 570cm^{-1} was strongly enriched in both decellularized SI and colonic scaffolds. This peak has previously been attributed to CO_2 rocking and the S-S bridge of cysteine, proline and tryptophan that are likely the characteristics of the ECM[39]. Similarly, the peak at 1418cm^{-1}, which is attributed to CH_2 bending mode of proteins and lipids, was also detected in the decellularized scaffolds. The enrichment of these two peaks in the decellularized scaffolds highlights the unique properties of the structural ECM scaffolds that lack a dense cell population. Interestingly, minimal difference in peak intensity of the spectra profile was observed between native and decellularized scaffolds in the submucosal region that contains the least cellular density, suggesting that the main difference between the native and decellularized tissues is likely due to the removal of the cellular mass rather than the DET process itself. Of note, the overall spectra profiles between SI and colonic scaffolds were highly analogous, suggesting that the biochemical composition is largely conserved between SI and colonic scaffolds. To demonstrate the spatial distribution of intestinal ECM components in the decellularized scaffolds, Raman spectroscopy was further used for grouping spectra with a similar profile and visualizing their spatial localization via Raman heatmaps. In particular, we noted that collagen was mainly localized to the submucosal layer, while phenylalanine - indicating most proteinaceous regions - was most abundant in the muscularis propria (Fig. 3b). On the other hand, glycosaminoglycans (GAGs), indicated by glucosamines spectra, were highly enriched in the mucosal layer (Fig. 3b). Consistent to the spectra profiling, the ECM component distributions were also highly similar between SI and colonic scaffolds. The results highlight the distinct biomolecular compositions for each histological layer of the scaffolds after decellularization process, which offer essential structural and biochemical cues for cellular reconstitution. Principal component analysis of the spectra profiles readily segregated the spectra into distinct clusters based on their layer identities (Fig. 3c). Remarkably, the mucosal spectra of both SI and colonic scaffold was tightly clustered together, which was distinct from the submucosal muscularis spectra which are positively characterized (Fig. 3c and Supplementary Fig. 2a). The data suggest that the biochemical composition of the mucosal layer from both SI and colon are more similar to each other than their corresponding deeper histological layers of the scaffolds. To further characterize the biomolecular profiles, mass spectrometry was used to generate a global proteomic profile of the decellularized SI and colonic ECM scaffolds (n=4 each). This revealed a total of 377 proteins detected in the scaffolds, among which 126 were ECM proteins (Supplementary Table 2). Strikingly, majority of the proteins were detected in both SI and colonic scaffolds, while only 11/377 total proteins and 2/126 ECM proteins were detectable in either SI or colonic scaffolds
(Fig. 3d). These included 17 collagen subtypes and 5 Laminin subtypes (Supplementary Table 3). Among the 2 ECM proteins, Defensin-5A (DEFA5) was detectable only in SI scaffold while Thrombospondin-4 (THBS4) was detectably only in colonic scaffolds. Immunohistochemical staining confirmed the restricted expression of DEFA5 in SI but not colon, which was secreted by SI-specific Paneth cells (Supplementary Fig. 2b). THBS4, on the other hand, was expressed in both native SI and colon (Supplementary Fig. 2c), suggesting that the difference noted in mass spectrometry might be due to the detection limit in the SI ECM scaffolds rather than actual expression difference. Altogether, comprehensive analysis of the proteomic profiles of the decellularized intestinal scaffolds

demonstrate the highly analogous biochemical composition between human SI and colonic matrix, implicating that both can potentially be used for jejunal graft reconstruction.

***In vitro* reconstruction of jejunal mucosal grafts**

To enhance the bioengineering efficiency, we further generated primary human intestinal fibroblasts isolated from the same intestinal tissues used to derive organoids or SI scaffolds (Supplementary Table 1). Primary human intestinal fibroblasts could be cultured and expanded for up to 10 passages while retaining strong expression of typical stromal matrix markers fibronectin, vimentin, fibroblast surface protein marker-1, laminin α5 and with scattered weaker co-expression of αSMA (Supplementary Fig. 3). This indicates a mixed population of intestinal fibroblasts and
11 myofibroblasts, which are both essential stromal niche for the sur 227 vival and maintenance of hISCs. To reconstruct a jejunal graft, primary human intestinal fibroblasts were first injected into the scaffolds at the mucosal-submucosal boundary and maintained in static culture for 3 days to recreate the native microenvironment (Fig. 4a). Primary human jejunal organoids were subsequently seeded onto the luminal surface of the scaffold, which was mounted on a customized scaffold holder. The mounted graft was maintained under static conditions for another 4 days, which was then transferred to a dynamic culture condition using a perfusion bioreactor (Fig. 4a). The grafts were maintained under dynamic conditions for at least 14 days before *in vivo* transplantation or histological analysis. Human jejunal organoids were seeded on piglet SI scaffolds for initial optimization. Micro-CT imaging was performed on the seeded scaffolds to assess the volume and distribution of epithelial cells on the scaffold, which showed a full surface area coverage of the scaffold (Supplementary Fig. 4a). Histology analysis of the reconstructed grafts showed an organized monolayer of columnar cells on the scaffold (Supplementary Fig. 4b). Regions of collagen-positive new matrix deposition were detected with structures resembling new villi (Supplementary Fig. 4b,c). In addition, all intestinal cell types were readily detected in the graft, including lysozyme-positive Paneth cells, AB-PAS-positive goblet cells and alkaline phosphatase/ALPI-positive enterocytes (Supplementary Fig. 4d-f). Importantly, the jejunal-specific enzyme sucrase isomaltase was also broadly detected on the brush boarder of the epithelial cells, indicating that the region-specific identity was preserved in the engineered graft (Supplementary Fig. 4g). Proliferation marker Ki67 was also detected in the graft (Supplementary Fig. 4h).

Next, we examined the graft reconstruction and differentiation potential by seeding human jejunal organoids on human SI or colonic scaffolds. Similar to piglet scaffold data, histology analysis revealed a continuous monolayer of columnar epithelial cells distributed evenly along the decellularized human SI scaffold surfaces (Fig. 4b). Immunostaining confirmed that proliferation (as indicated by PCNA) and differentiation (ALPI to mark enterocytes and AB-PAS to mark goblet cells) 12potential was maintained in the reconstructed 253 grafts. Electron microscopy analysis further demonstrated the presence of microvilli (brush boarder of enterocytes), basement membrane (as indicated by basal lamina and reticular lamina features between the scaffold and the epithelial cells), goblet cell mucous vesicles and Paneth cell secretory vesicles (Fig. 4d). Tight junction (ZO1) and polarity (Na+/K+/ATPase) markers were also expressed on the reconstructed jejunal scaffold (Fig. 4e). The presence of basement membrane and junction markers is encouraging as they are essential for the barrier function of the intestine. Interestingly, immunofluorescent staining of collagen showed new matrix deposition in multiple regions underneath the epithelial cells, suggesting ECM remodeling mediated by epithelial cells (Fig. 4b). Similar jejunal graft reconstruction results were observed using human colonic ECM scaffold, where proliferation, differentiation and ECM remodeling were all detected (Fig. 4c). Importantly, the SI-specific expression of ALPI was also detected on the seeded colonic scaffold (Fig. 4c), suggesting that both human SI and colonic ECM scaffolds can be used as biological platforms for reconstruction of jejunal grafts with full proliferation and differentiation potential. Together, the results indicate that human jejunal grafts can be

robustly regenerated using either piglet, human SI or colonic scaffolds with capacity for absorptive, digestive and barrier function.

***Ex vivo* functional analysis of the engineered jejunal grafts**

Next, we examined the absorptive and digestive function of the bioengineered grafts at different time points of culture (Fig. 5a). First, the absorptive capacity of the reconstructed jejunal grafts was tested at day 18 of culture by adding the fluorescently labelled peptide β-Ala-Lys-AMCA to the culture. Immunofluorescent staining confirmed the presence of β-AMCA peptides in the epithelial cells, indicating that the engineered graft possesses peptide absorptive function (Fig. 5b). Plasma citrulline levels positively correlate to enterocyte mass and absorptive function and are used as a clinical biomarker of intestinal failure[40]. Citrulline levels were measured in the bioreactor circuit at day 0, day 11 and day 25 of culture as a surrogate marker of enterocyte growth on the scaffolds.

13 There was a continuous increase in citrulline concentrations from 278 day 0 to day 25 in the jejunal grafts regenerated in all three scaffold types, implicating the formation of healthy functional enterocytes in all constructs (Fig. 5c). To further demonstrate digestive function of the reconstructed jejunal grafts, we examined the jejunal enterocyte brush border enzyme sucrase isomaltase function by challenging the constructs with sucrose and measuring the glucose (one of the metabolic products) production at various time point of the culture. Remarkably, glucose production was detected as early as day 4 culture in all three scaffold types, indicating that the disaccharidase function of the jejunal grafts are present throughout the *ex vivo* culture (Fig. 5d). The findings confirmed the presence of absorptive and digestive functions of the engineered human jejunal grafts regenerated on all ECM scaffold types.

***In vivo* transplantation of the engineered jejunal grafts**

To examine the survival and maturation of the engineered jejunal grafts *in vivo*, we further transplanted the grafts in immunodeficient mice under the kidney capsule or in subcutaneous pockets that present different *in vivo* microenvironments regarding stromal infiltration and vascularization. First, the jejunal grafts seeded on piglet scaffolds were collected at Day 18 of the culture and transplanted under kidney capsule. Engrafted engineered intestine was collected 7 days after transplantation, which showed signs of neo-vascularization macroscopically surrounding the scaffold (Fig. 6a). Serial histological sectioning along the length of the scaffold demonstrated the presence of continuous rings of intestinal epithelium that were positive for human nucleoli staining (Fig. 6b,c and Supplementary Fig. 5a). 3D volume reconstruction of the serial histological section data revealed segments of continuous tubular structures maintained throughout the graft, indicating formation of intestinal lumens (Fig. 6d, movie 1). Surprisingly, immunostaining of AB-PAS and ALPI was largely negative in the graft, suggesting a lack of goblet cell and enterocyte differentiation in the engineered graft after engraftment to kidney capsule (Supplementary Fig. 5b). Interestingly, a large population of cells co-expressed with vimentin and αSMA was noted surrounding the lumen, 14 indicating that there is a strong infiltration of host myofibroblasts 303 into the scaffold (Fig. 6e).

Immunofluorescent staining further demonstrated high expression of stem cell markers OLFM4 and SOX9 (Fig. 6f,g). Together, the results suggest that transplantation of the jejunal graft in kidney capsule drives the intestinal epithelium to undifferentiated state, which could be due to the strong stromal infiltration that recapitulates the microenvironment of the intestinal stem cell niche. Since kidney capsule transplantation was technically challenging for human scaffolds due to the significant thickness of the constructs, we proceeded to test subcutaneous implantation approach that allows engraftment of larger human scaffold constructs. We further pre-labelled the human jejunal organoids with a GFP-luciferase reporter prior to *in vitro* seeding, which enabled us to monitor the epithelial growth *in vivo* with live bioluminescent imaging (Fig. 6h). We first repeated the transplantation experiment using jejunal grafts seeded on piglet scaffolds subcutaneously for comparison. Similar to kidney capsule model, lumens of human nucleoli-positive

intestinal epithelial cells were readily detected as soon as 7 days after implantation (Fig. 6i). However, unlike kidney capsule data, ALPI+ enterocytes and AB-PAS+ goblet cells were detected in the graft with significantly less stromal infiltration (Fig. 6i). We postulate that the low stromal infiltration during subcutaneous engraftment may offer a better approach to allow functional differentiation of the jejunal grafts.

Next, we performed subcutaneous transplantation of the jejunal grafts that were seeded on human scaffolds. In order to enhance the growth of ectopically transplanted jejunal grafts in this model, we further investigated the potential use of the drug Teduglutide for tissue engineering applications. Teduglutide is clinically licensed for use in patients with intestinal failure to promote intestinal adaptation by increasing villus height and crypt depth[41]. Since the receptor (GLP2R) of

Teduglutide was expressed in both human fibroblasts and organoids (Supplementary Fig. 5c), we decided to treat the mice with Teduglutide during *in vivo* transplantation. Similar to piglet scaffold data, jejunal graft with human scaffold was also able to form lumen after transplantation

15 (Supplementary Fig. 5d). Human SI 328 scaffold was significantly thicker than piglet ones, where the three histological layers (mucosa, submucosa and muscularis) of the graft were clearly preserved after transplantation (Fig. 6j). A distinctive monolayer of human intestinal epithelial cells was formed on the mucosal luminal surface of the implanted scaffold. Proliferating cells (indicated by PCNA and Edu staining) were detected in both epithelial and pericryptal stromal cells of the scaffold (Fig. 6k). Electron microscopy analysis identified mucous granules within the graft epithelial cells, suggesting the presence of early goblet cell differentiation (Fig. 6l). Immunofluorescent staining of human specific pancytokeratin and e-cadherin confirmed the epithelial identity of the cells (Fig. 6m,n). Expression of human-specific stromal marker vimentin further confirmed the survival of human intestinal fibroblasts in the injected grafts after transplantation (Fig. 6m). Importantly, the jejunal specific brush border enzyme sucrase isomaltase was broadly expressed in majority of the jejunal graft (Fig. 6n), indicating that human ECM scaffold supports and maintains intestinal epithelial cell differentiation towards enterocyte lineage *in vivo*.

Recent advances of organoid culture have opened up exciting avenues for regenerative medicine. However, the regenerative potential of organoids is limited to small lesions only, while larger-scale tissue damage such as organ failure would require more sophisticated approaches. Tissue engineering offers promising alternative treatment strategy for patients with organ failure. However, engineering of complex organs such as intestine is still far from clinical translation due to the limited supportive evidence from pre-clinical studies. Establishment of a robust and relevant protocol for timely organ reconstruction using patient-derived human materials is a critical step prior translation. In the current study, we described a robust protocol to isolate and expand primary hISCs from children with IF. The ability to rapidly derive and expand autologous hISCs and stromal cells from little biopsies is crucial for IF children with very limited residual intestine. We also confirmed that the primary SI organoids retained their region-specific identities and differentiation capacity after pro-longed culture under expansion conditions. Importantly, these primary SIorganoids can robustly repopulate the decellularized intestine in customized bioreactors and develop appropriate absorptive and digestive function, which can further survive and mature *in vivo*. To our knowledge, this is the first pre-clinical study that describes protocol for robust generation of primary human SI organoids and decellularized scaffolds from IF patients for jejunal graft reconstruction. Previous work on tissue engineering of small intestine focused mainly on either synthetic scaffolds or ECM scaffolds derived from rodent and porcine. A recent study reported tissue engineering of small intestine using ESC-derived hIOs. The authors showed that the survival and intestinal fate were only maintained when these hIOs were seeded on artificial polyglycolic/poly L lactic acid scaffolds but not on decellularized ECM scaffolds. Their results raised concerns on the clinical application of decellularized ECM scaffold for intestinal tissue engineering.

One plausible explanation of the data is that ESC-derived hIOs may not be the ideal cell source for tissue engineering using decellularized ECM scaffold, possibly due to epigenetic plasticity induced during reprogramming. Unlike many other previous tissue engineering studies that focused on iPSCs, 17 synthetic scaffolds or rodent ECM matrix, the use of primary human 368 materials (both cells and decellularized ECM matrix) in this study is a highly relevant step towards clinic translation. Our findings further suggest that routine banking of intestinal epithelial organoids and stromal cells may conceivably be introduced as a new clinical standard at the point of intestinal resections in infants and children undergoing bowel resection (e.g. necrotizing enterocolitis) to facilitate personalized intestinal reconstruction in the future. The DET decellularization protocol represents a more physiological approach for the fabrication of non-immunogenic biological scaffolds as compared to synthetic polymers. The ability to preserve the biological and structural features of the decellularized scaffolds after cryopreservation further suggests the potential of these scaffolds to become “off-shelf” clinical products[13]. Previous studies have demonstrated the conservation of the biological ECM molecules (e.g. collagen and GAGs) in rodent or piglet intestinal scaffolds using targeted methods such as immunohistochemical staining of the tissues. Here, we characterized the ultrastructure and biochemical composition of the human derived intestinal scaffolds comprehensively and unbiasedly using electron microscopy, Raman spectroscopy and mass spectrometry[50]. Raman imaging demonstrated that the global biomolecular cues amongst the histological layers were largely conserved between the native and decellularized scaffolds. Moreover, spectral signatures arising from the human SI and colon scaffolds were remarkably analogous. This was further supported by the unbiased mass spectrometry analysis that showed highly conserved global and ECM protein profiles despite significant microarchitectural differences at the mucosal layer (i.e. crypt-villus units in the SI scaffold as compared to the lack of villi in the colonic scaffold). Importantly, we demonstrated that human jejunal organoids were able to engraft, proliferate, differentiate and function appropriately on both human SI and colon ECM scaffolds with jejunal-specific brush border enzyme expression and ECM remodeling, suggesting that the intestinal epithelia have cell-intrinsic role in defining the region-specific identity. Our findings support the potential use of colon scaffolds for SI graft reconstruction, which has strong clinical implications for two main reasons. Firstly, colon 18 derived from cadaveric donors or resected in children affected by 394 conditions such as Hirschsprung’s disease could be decellularized, stored, and donated for therapy. Secondly, in conditions such as midgut volvulus, in which typically the large bowel is preserved, there is the potential to convert the IF patient’s own colon to SI by replacing the mucosal layer with jejunal organoids as an alternative treatment solution. Finally, our data generated on piglet scaffolds suggest that porcine ECM matrix could also be used as for human organ reconstruction. In addition, we further demonstrated that the engineered jejunal grafts were structurally and functionally competent for cell engraftment and vascularization when transplanted *in vivo*. While the strong stromal infiltration during kidney capsule engraftment resulted in stem cell maintenance and lack of differentiation, grafts were well-differentiated in the subcutaneous implantation model. Intestinal stromal cells, including fibroblasts and myofibroblasts, are known to constitute the essential microenvironment for ECM remodeling and growth factors secretion for stem cell maintenance[51]. The results highlight the essential niche role of stromal cells for the survival and maintenance of the engineered grafts. These outcomes can also be enhanced *in vivo* by the drug teduglutide[52], which was used clinically in IF patients to increase villus height and crypt depth of the intestinal mucosa[53]. Our data showed that administration of teduglutide enhanced the survival of the subcutaneously transplanted intestinal grafts, a site with less host stromal infiltration of the scaffolds. Given that teduglutide is clinically approved for IF patients, we believe that its application during transplantation of the engineered intestinal grafts in IF patients may further promote survival and differentiation of the grafts *in vivo*.

4. Conclusions and future steps

In summary, the current study describes a robust protocol for the timely jejunal mucosal reconstruction using IF patient-derived primary materials including organoid, fibroblasts and ECM scaffolds. The next step will be to scale up the jejunal graft for pre-clinical testing in larger animal models using orthotopic transplantation. Our findings represent an important conceptual advance towards the reconstruction of full thickness of intestinal wall including the enteric neuromuscular cells that drive peristalsis along the length of the engineered 419 intestine for autologous transplantation to IF patients.

5. Bibliographical references

1. O'Keefe, S.J.*, et al.* Short bowel syndrome and intestinal failure: consensus definitions and overview. *Clin Gastroenterol Hepatol* 4, 6-10 (2006).

2. Goulet, O. & Ruemmele, F. Causes and management of intestinal failure in children. *Gastroenterology* 130, S16-28 (2006).

3. Cole, C.R., Hansen, N.I., Higgins, R.D., Ziegler, T.R. & Stoll, B.J. Very low birth weight preterm infants with surgical short bowel syndrome: incidence, morbidity and mortality, and growth outcomes at 18 to 22 months. *Pediatrics* 122, e573-582 (2008).

4. Vanderhoof, J.A. & Langnas, A.N. Short-bowel syndrome in children and adults. *Gastroenterology* 113, 1767-1778 (1997).

5. Martinez Rivera, A. & Wales, P.W. Intestinal transplantation in children: current status. *Pediatr Surg Int* 32, 529-540 (2016).

6. Martin, L.Y.*, et al.* Tissue engineering for the treatment of short bowel syndrome in children. *Pediatric research* 83, 249-257 (2018).

7. Quarta, M.*, et al.* Bioengineered constructs combined with exercise enhance stem cell mediated treatment of volumetric muscle loss. *Nature communications* 8, 15613 (2017).

8. Jank, B.J.*, et al.* Engineered composite tissue as a bioartificial limb graft. *Biomaterials* 61, 246-256 (2015).

9. Mazza, G.*, et al.* Decellularized human liver as a natural 3D-scaffold for liver bioengineering and transplantation. *Scientific reports* 5, 13079 (2015).

10. Uygun, B.E.*, et al.* Organ reengineering through development of a transplantable recellularized liver graft using decellularized liver matrix. *Nature medicine* 16, 814-820 (2010).

11. Zhou, H.*, et al.* Bioengineering Human Lung Grafts on Porcine Matrix. *Annals of surgery* 267, 590-598 (2018).

12. Ott, H.C.*, et al.* Regeneration and orthotopic transplantation of a bioartificial lung. *Nature medicine* 16, 927-933 (2010).

13. Urbani, L.*, et al.* Multi-stage bioengineering of a layered oesophagus with in vitro expanded muscle and epithelial adult progenitors. *Nature communications* 9, 4286 (2018).

14. Rama, P.*, et al.* Limbal stem-cell therapy and long-term corneal regeneration. *The New England journal of medicine* 363, 147-155 (2010).

15. Hirsch, T.*, et al.* Regeneration of the entire human epidermis using transgenic stem cells. *Nature* 551, 327-332 (2017).

16. Elliott, M.J.*, et al.* Stem-cell-based, tissue engineered tracheal replacement in a child: a 2- year follow-up study. *Lancet (London, England)* 380, 994-1000 (2012).

17. Atala, A., Bauer, S.B., Soker, S., Yoo, J.J. & Retik, A.B. Tissue-engineered autologous bladders for patients needing cystoplasty. *Lancet (London, England)* 367, 1241-1246 (2006).

18. Booth, C.C. The metabolic effects of intestinal resection in man. *Postgrad Med J* 37, 725-739 (1961).

19. Wales, P.W.*, et al.* Neonatal short bowel syndrome: population-based estimates of incidence and mortality rates. *J Pediatr Surg* 39, 690-695 (2004).

20. Stollman, N.H., Neustater, B.R. & Rogers, A.I. Short-bowel syndrome. *The Gastroenterologist* 4, 118-128 (1996).

21. Fattahi, F.*, et al.* Deriving human ENS lineages for cell therapy and drug discovery in Hirschsprung disease. *Nature* 531, 105-109 (2016).

22. Hong, S.N., Dunn, J.C., Stelzner, M. & Martin, M.G. Concise Review: The Potential Use of Intestinal Stem Cells to Treat Patients with Intestinal Failure. *Stem cells translational medicine* 6, 666-676 (2017).

23. Clevers, H.*, et al.* Tissue-Engineering the Intestine: The Trials before the Trials. *Cell stem cell* 24, 855-859 (2019).

24. Ben-David, U. & Benvenisty, N. The tumorigenicity o 812 f human embryonic and induced pluripotent stem cells. *Nature reviews. Cancer* 11, 268-277 (2011).

25. Liang, G. & Zhang, Y. Genetic and epigenetic variations in iPSCs: potential causes and implications for application. *Cell stem cell* 13, 149-159 (2013).

26. Laurent, L.C.*, et al.* Dynamic changes in the copy number of pluripotency and cell proliferation genes in human ESCs and iPSCs during reprogramming and time in culture. *Cell stem cell* 8, 106-118 (2011).

27. Hussein, S.M.*, et al.* Copy number variation and selection during reprogramming to pluripotency. *Nature* 471, 58-62 (2011).

28. Gore, A.*, et al.* Somatic coding mutations in human induced pluripotent stem cells. *Nature* 471, 63-67 (2011).

29. Sato, T.*, et al.* Long-term expansion of epithelial organoids from human colon, adenoma, adenocarcinoma, and Barrett's epithelium. *Gastroenterology* 141, 1762-1772 (2011).

30. Yui, S., *et al.* Functional engraftment of colon epithelium expanded in vitro from a single adult Lgr5(+) stem cell. *Nature medicine* 18, 618-623 (2012).

31. Costello, C.M., *et al.* Synthetic small intestinal scaffolds for improved studies of intestinal differentiation. *Biotechnology and bioengineering* 111, 1222-1232 (2014).

32. Chen, Y., *et al.* Robust bioengineered 3D functional human intestinal epithelium. *Scientific reports* 5, 13708 (2015).

33. Shaffiey, S.A., *et al.* Intestinal stem cell growth and differentiation on a tubular scaffold with evaluation in small and large animals. *Regenerative medicine* 11, 45-61 (2016).

34. Totonelli, G., *et al.* A rat decellularized small bowel scaffold that preserves villus-crypt architecture for intestinal regeneration. *Biomaterials* 33, 3401-3410 (2012).

35. Lee, E., Milan, A., Urbani, L., De Coppi, P. & Lowdell, M.W. Decellularized material as scaffolds for tissue engineering studies in long gap esophageal atresia. *Expert opinion on biological therapy* 17, 573-584 (2017).

36. Borgstrom, B., Dahlqvist, A., Lundh, G. & Sjovall, J. Studies of intestinal digestion and absorption in the human. *The Journal of clinical investigation* 36, 1521-1536 (1957).

37. Kitano, K., *et al.* Bioengineering of functional human induced pluripotent stem cell-derived intestinal grafts. *Nature communications* 8, 765 (2017).

38. Finkbeiner, S.R., *et al.* Generation of tissue-engineered small intestine using embryonic stem cell-derived human intestinal organoids. *Biology open* 4, 1462-1472 (2015).

39. Movasaghi, Z., Rehman, S. & Rehman, I.U. Raman Spectroscopy of Biological Tissues. *Applied Spectroscopy Reviews* 42, 493-541 (2007).

40. Fragkos, K.C. & Forbes, A. Citrulline as a marker of intestinal function and absorption in clinical settings: A systematic review and meta-analysis. *United European gastroenterology journal* 6, 181-191 (2018).

41. Kochar, B. & Herfarth, H.H. Teduglutide for the treatment of short bowel syndrome - a safety evaluation. *Expert opinion on drug safety* 17, 733-739 (2018).

42. Workman, M.J., *et al.* Engineered human pluripotent-stem-cell-derived intestinal tissues with a functional enteric nervous system. *Nature medicine* 23, 49-59 (2017).

43. Tuveson, D. & Clevers, H. Cancer modeling meets human organoid technology. *Science (New York, N.Y.)* 364, 952-955 (2019).

44. Fujii, M., Clevers, H. & Sato, T. Modeling Human Digestive Diseases With CRISPR-Cas9- Modified Organoids. *Gastroenterology* 156, 562-576 (2019).

45. Li, V.S. & Clevers, H. In vitro expansion and transplantation of intestinal crypt stem cells. *Gastroenterology* 143, 30-34 (2012).

46. Schweinlin, M., *et al.* Development of an Advanced Primary Human In Vitro Model of the Small Intestine. *Tissue engineering. Part C, Methods* 22, 873-883 (2016)

47. Grant, C.N.*, et al.* Human a 861 nd mouse tissue-engineered small intestine both demonstrate digestive and absorptive function. *American journal of physiology. Gastrointestinal and liver physiology* 308, G664-677 (2015).

48. Choi, R.S.*, et al.* Studies of brush border enzymes, basement membrane components, and electrophysiology of tissue-engineered neointestine. *J Pediatr Surg* 33, 991-996; discussion 996-997 (1998).

49. Ladd, M.R.*, et al.* Development of Intestinal Scaffolds that Mimic Native Mammalian Intestinal Tissue. *Tissue engineering. Part A* (2019).

50. Kallepitis, C.*, et al.* Quantitative volumetric Raman imaging of three dimensional cell cultures. *Nature communications* 8, 14843 (2017).

51. Meran, L., Baulies, A. & Li, V.S.W. Intestinal Stem Cell Niche: The Extracellular Matrix and Cellular Components. *Stem cells international* 2017, 7970385 (2017).

52. Kim, E.S. & Keam, S.J. Teduglutide: A Review in Short Bowel Syndrome. *Drugs* 77, 345-352 (2017).

53. Jeppesen, P.B., Gabe, S.M., Seidner, D.L., Lee, H.M. & Olivier, C. Factors Associated With Response to Teduglutide in Patients With Short-Bowel Syndrome and Intestinal Failure.*Gastroenterology* 154, 874-885 (2018).

54. Naba, A.*, et al.* The matrisome: in silico definition and in vivo characterization by proteomics of normal and tumor extracellular matrices. *Molecular & cellular proteomics : MCP* 11, M111.014647 (2012).

55. Lieber, C.A. & Mahadevan-Jansen, A. Automated method for subtraction of fluorescence from biological Raman spectra. *Applied spectroscopy* 57, 1363-1367 (2003).

56. Boyde, T.R. & Rahmatullah, M. Optimization of conditions for the colorimetric determination of citrulline, using diacetyl monoxime. *Analytical biochemistry* 107, 424-431 (1980).

57. Cardona, A.*, et al.* TrakEM2 software for neural circuit reconstruction. *PloS one* 7, e38011 (2012).

6. Figures

Figure 1

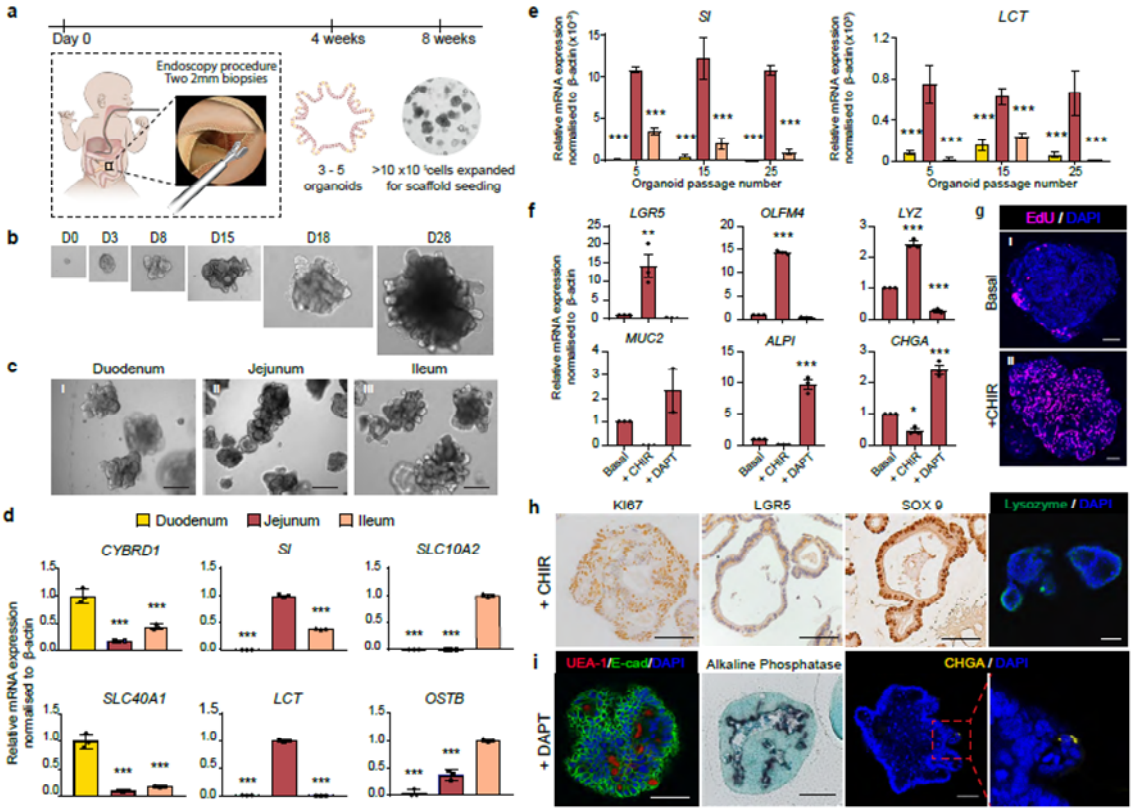

Figure 2

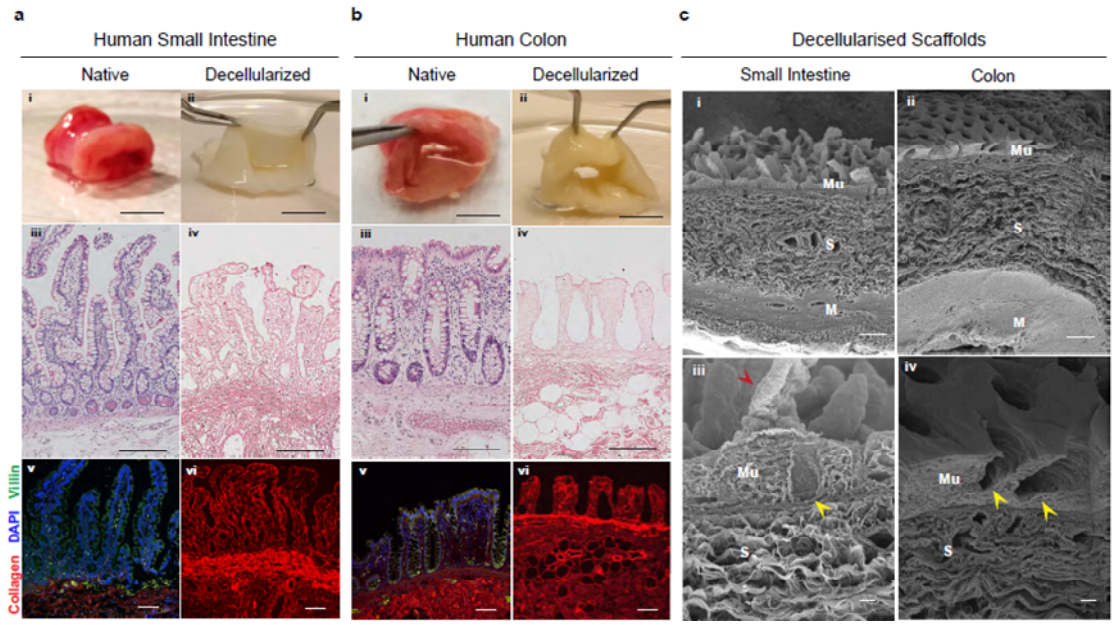

Figure 3

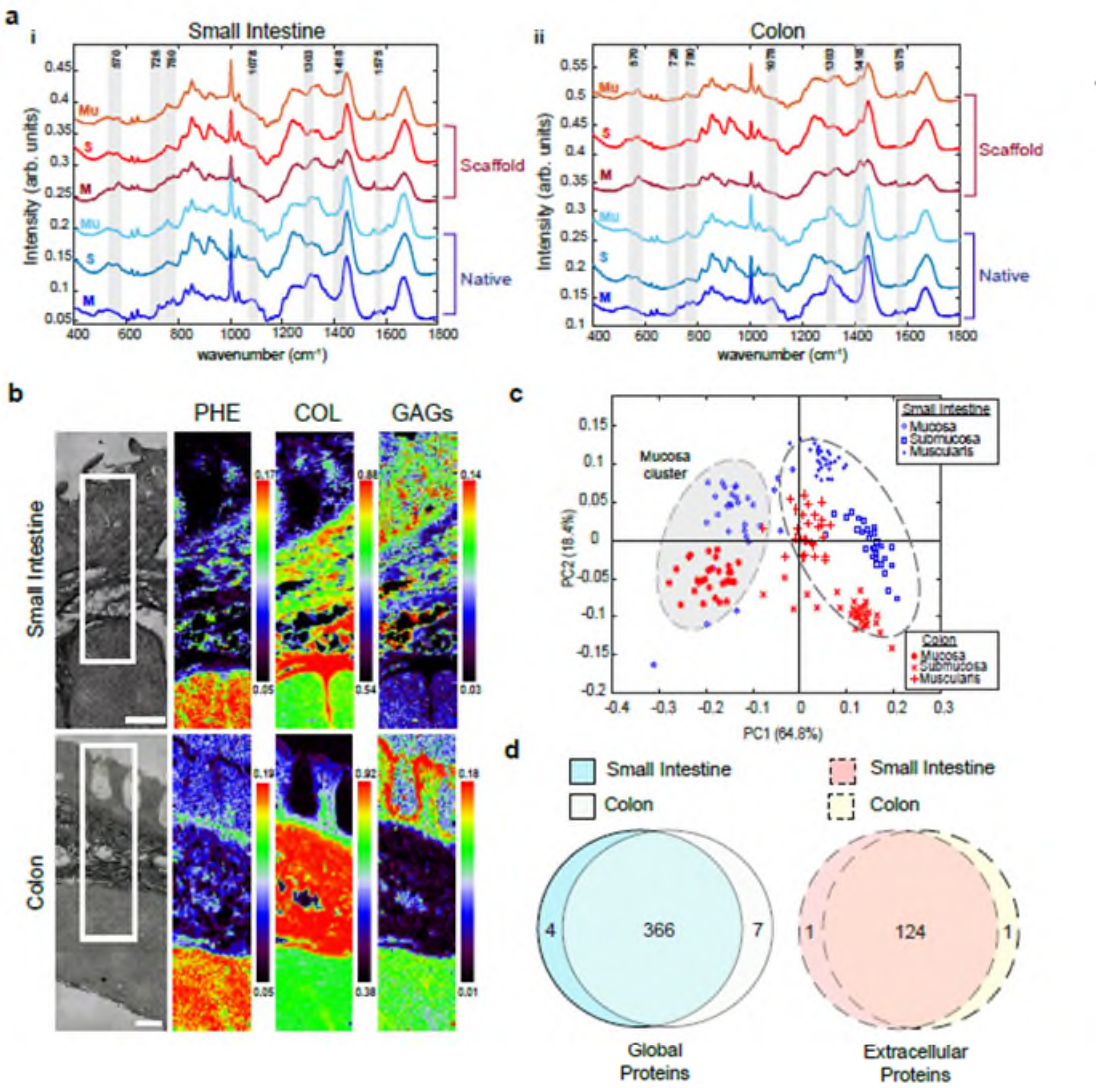

Figure 4

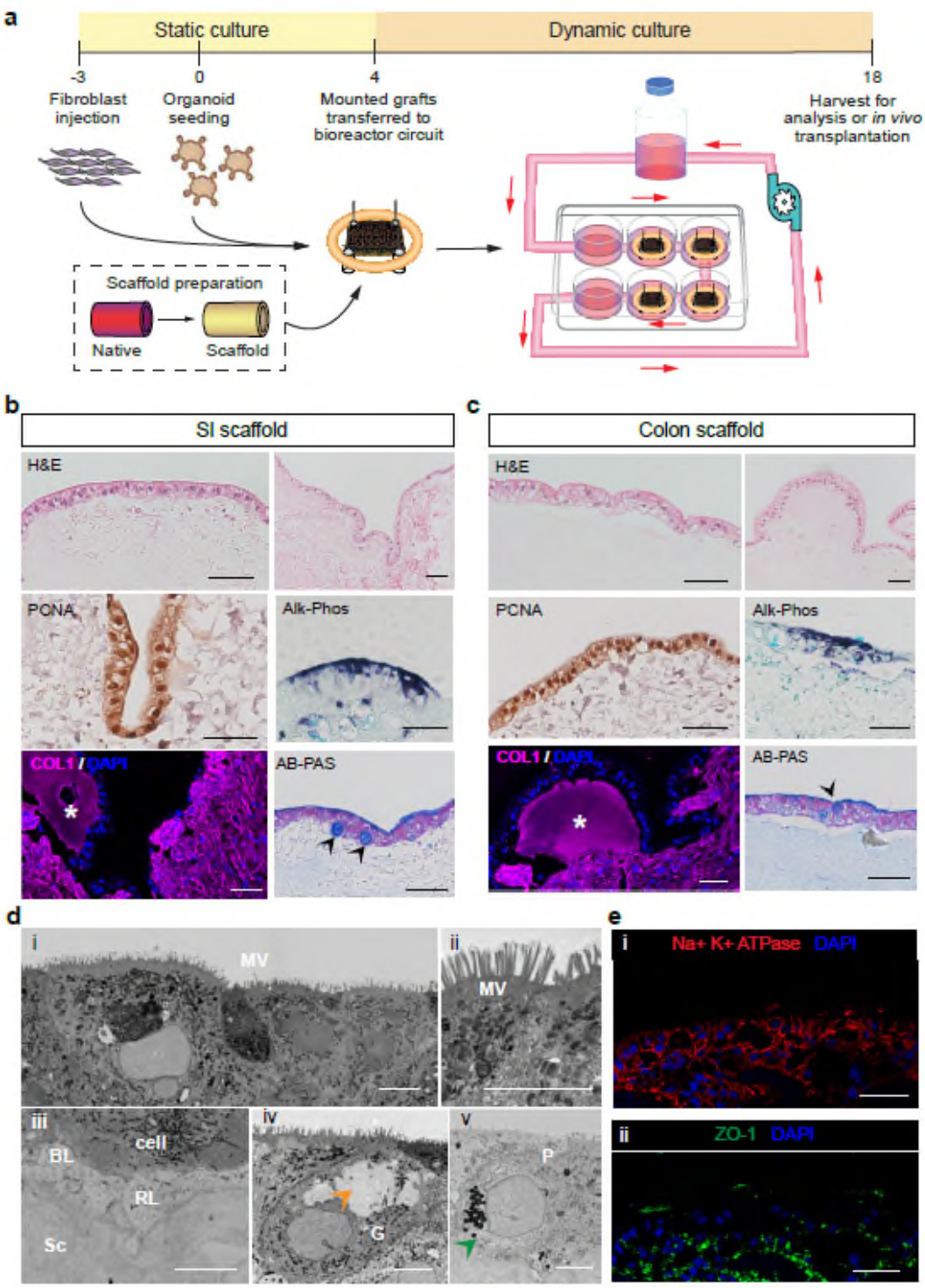

Figure 5

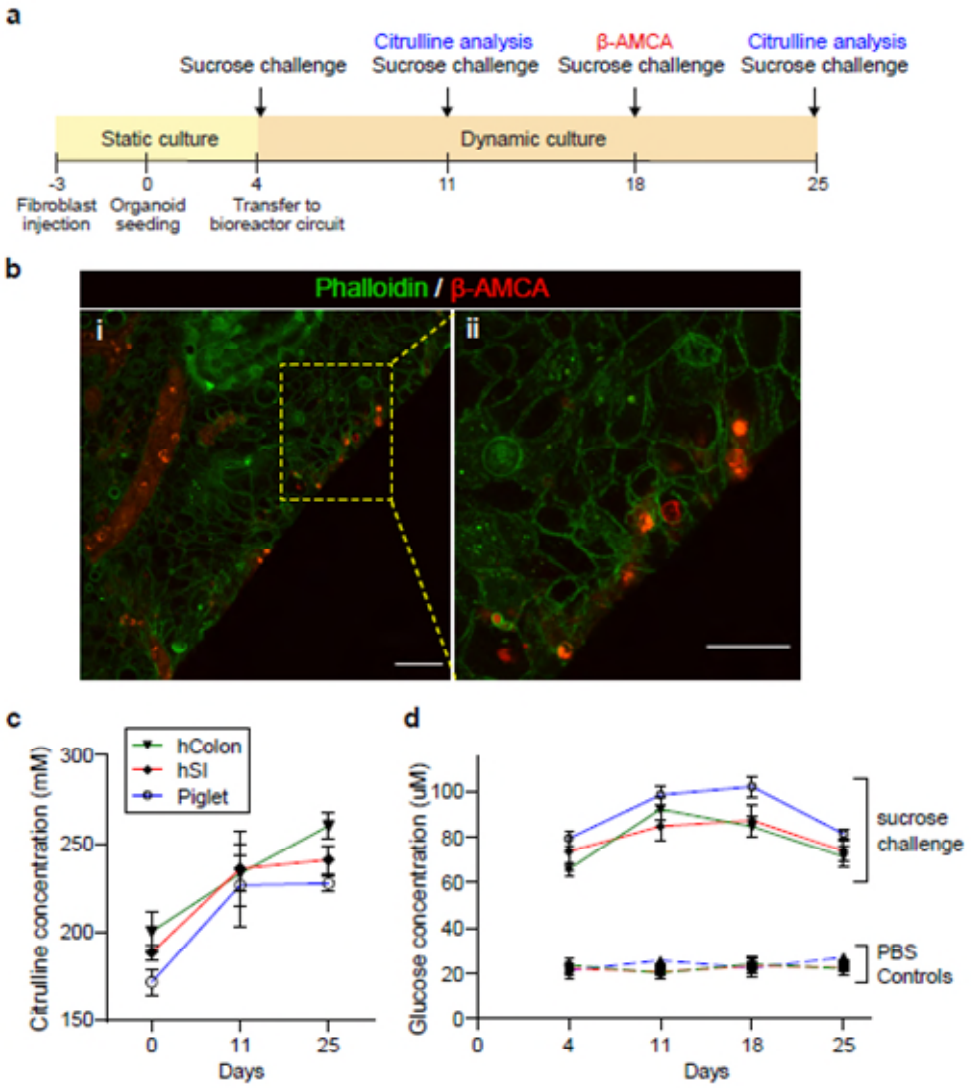

Figure 6

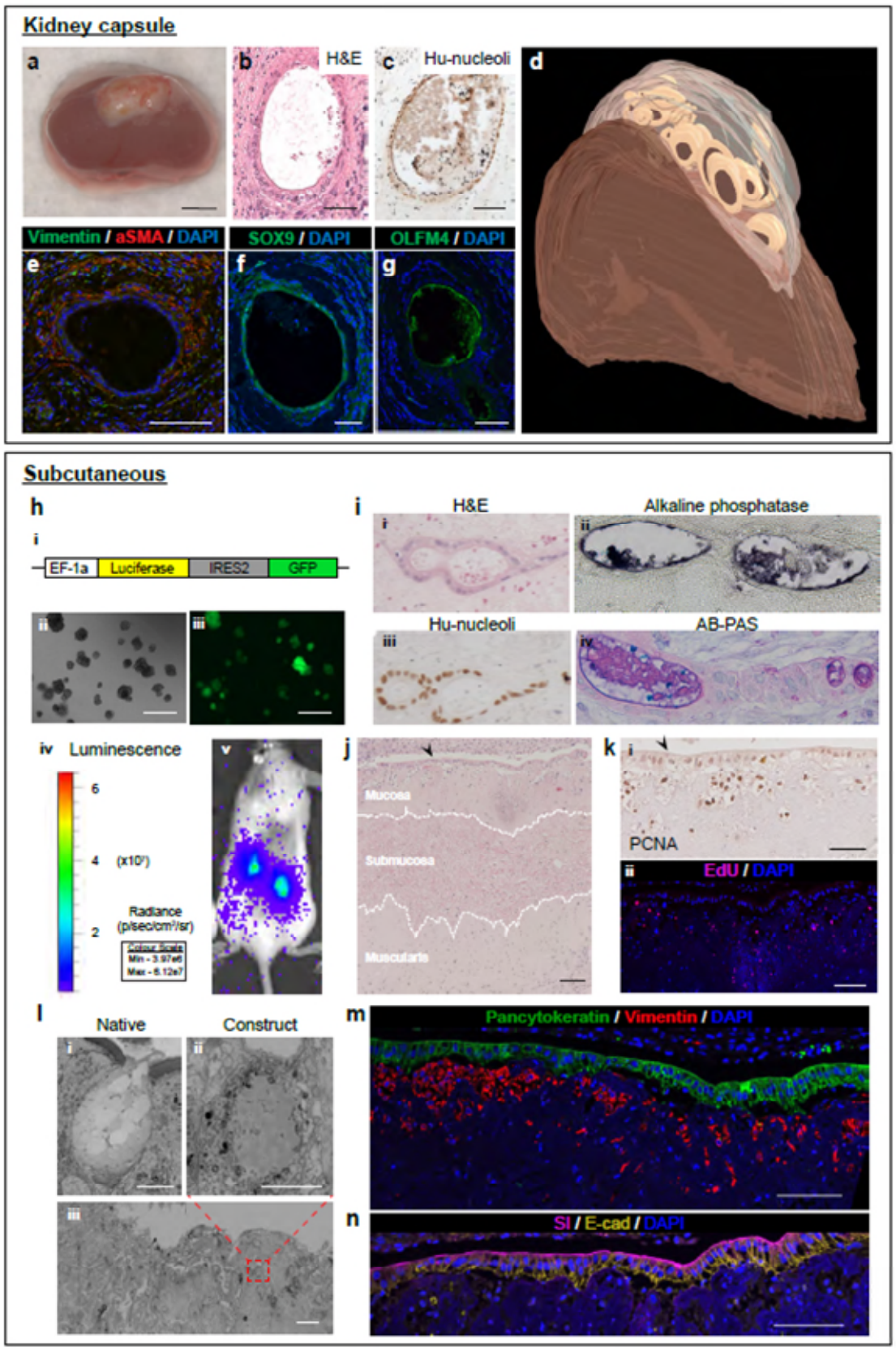

Supplementary Figure 1

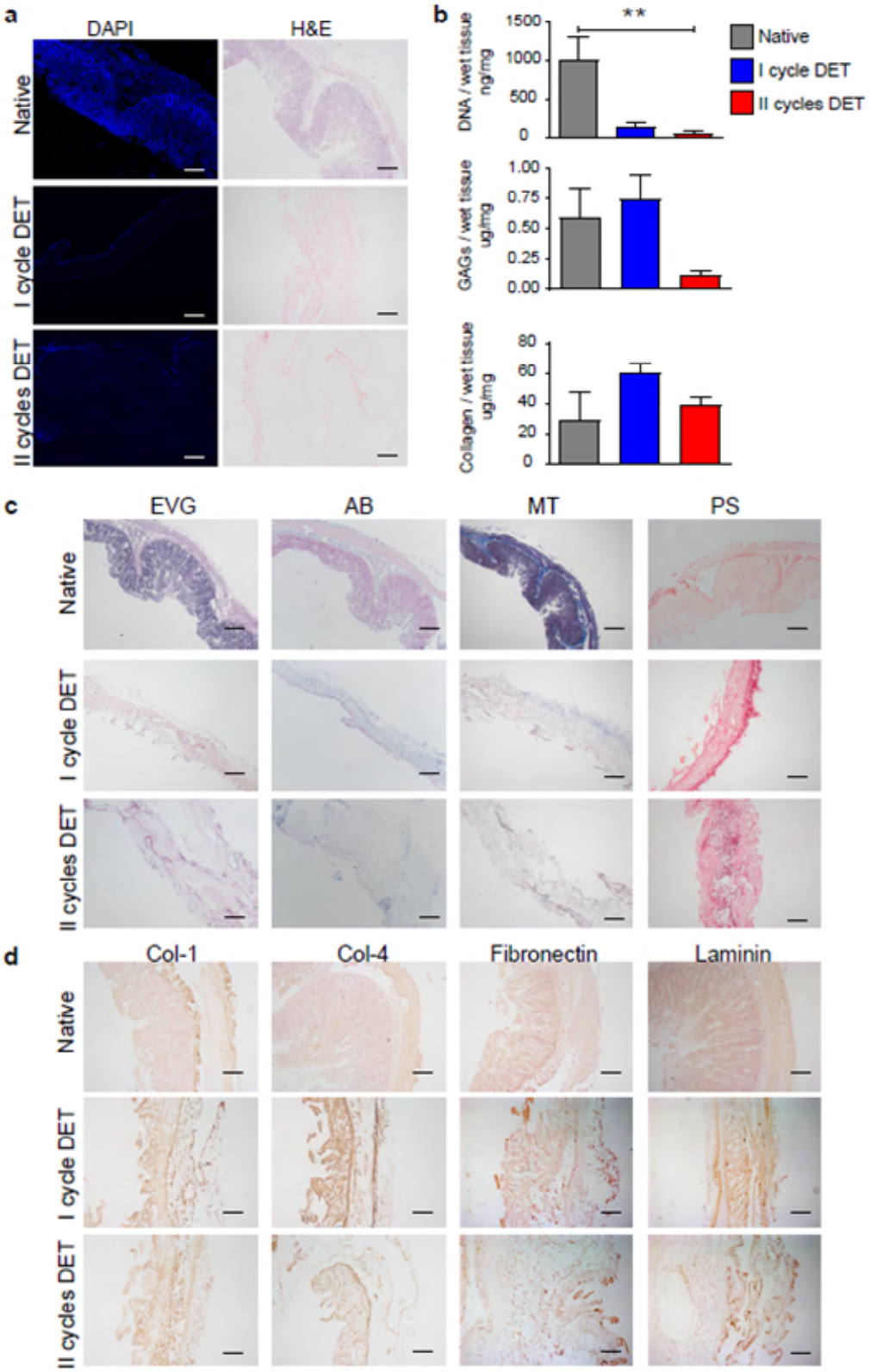

Supplementary Figure 2

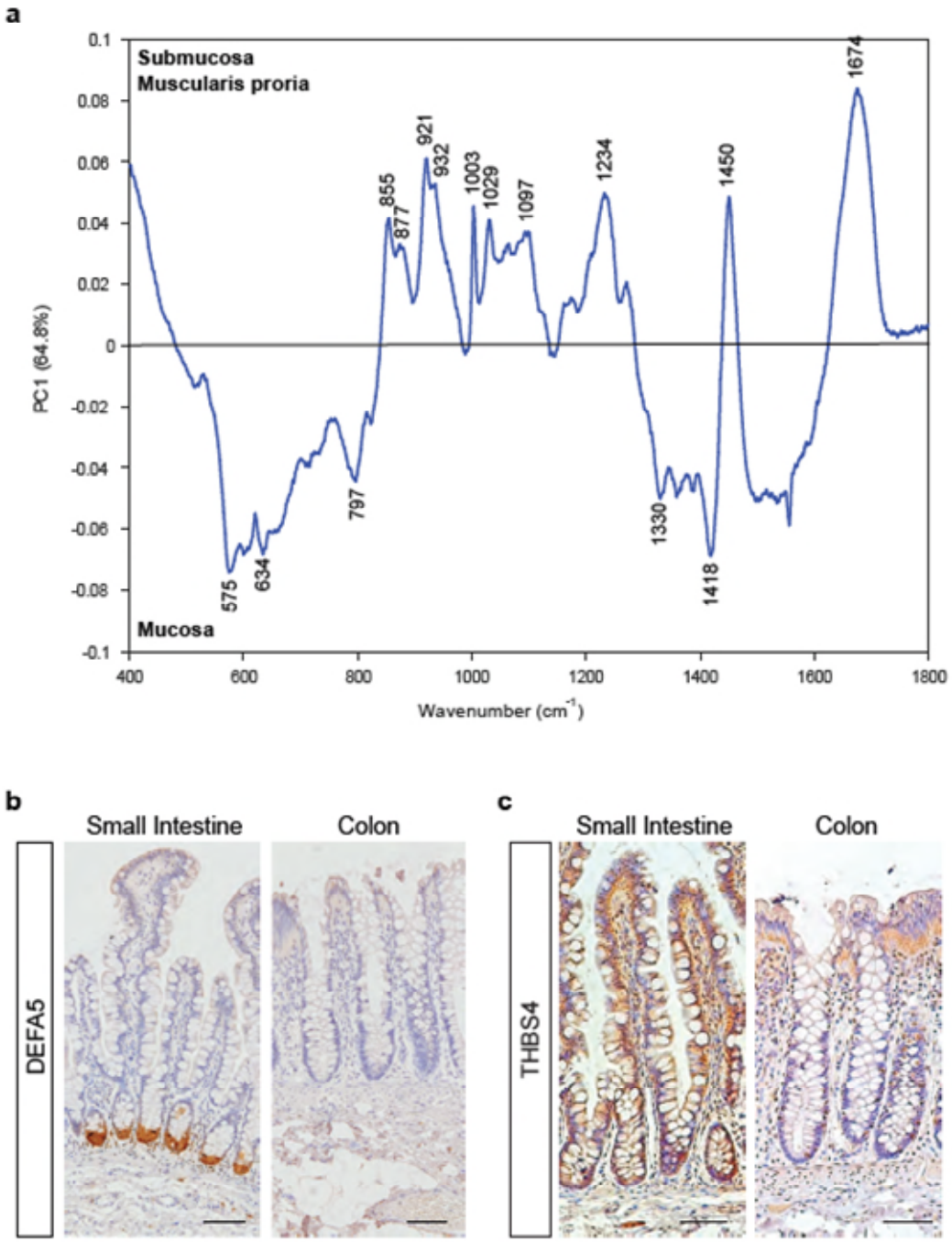

Supplementary Figure 3

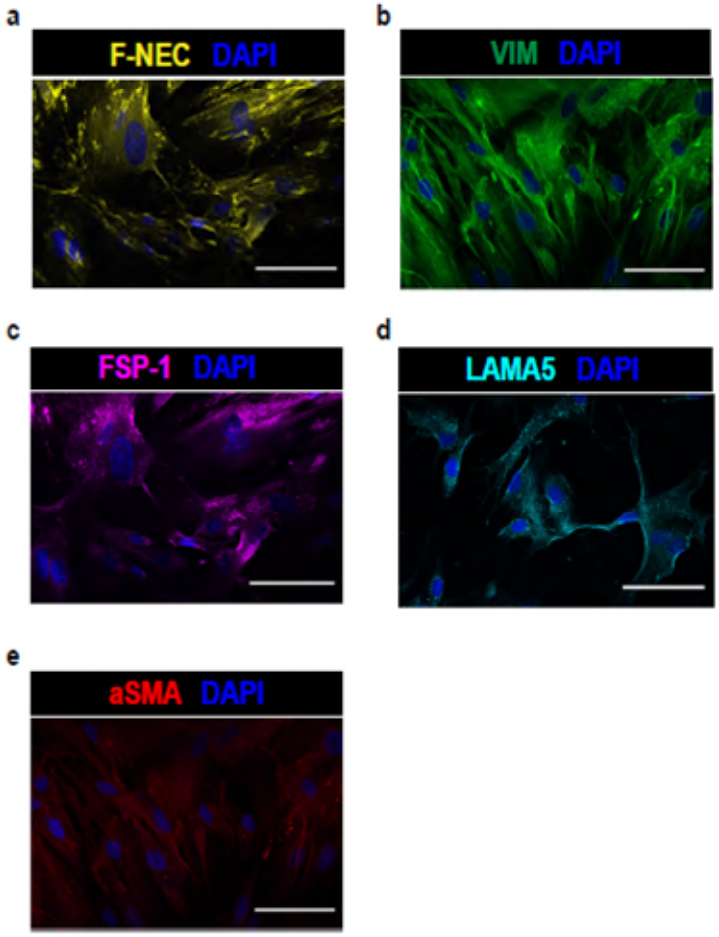

Supplementary Figure 4

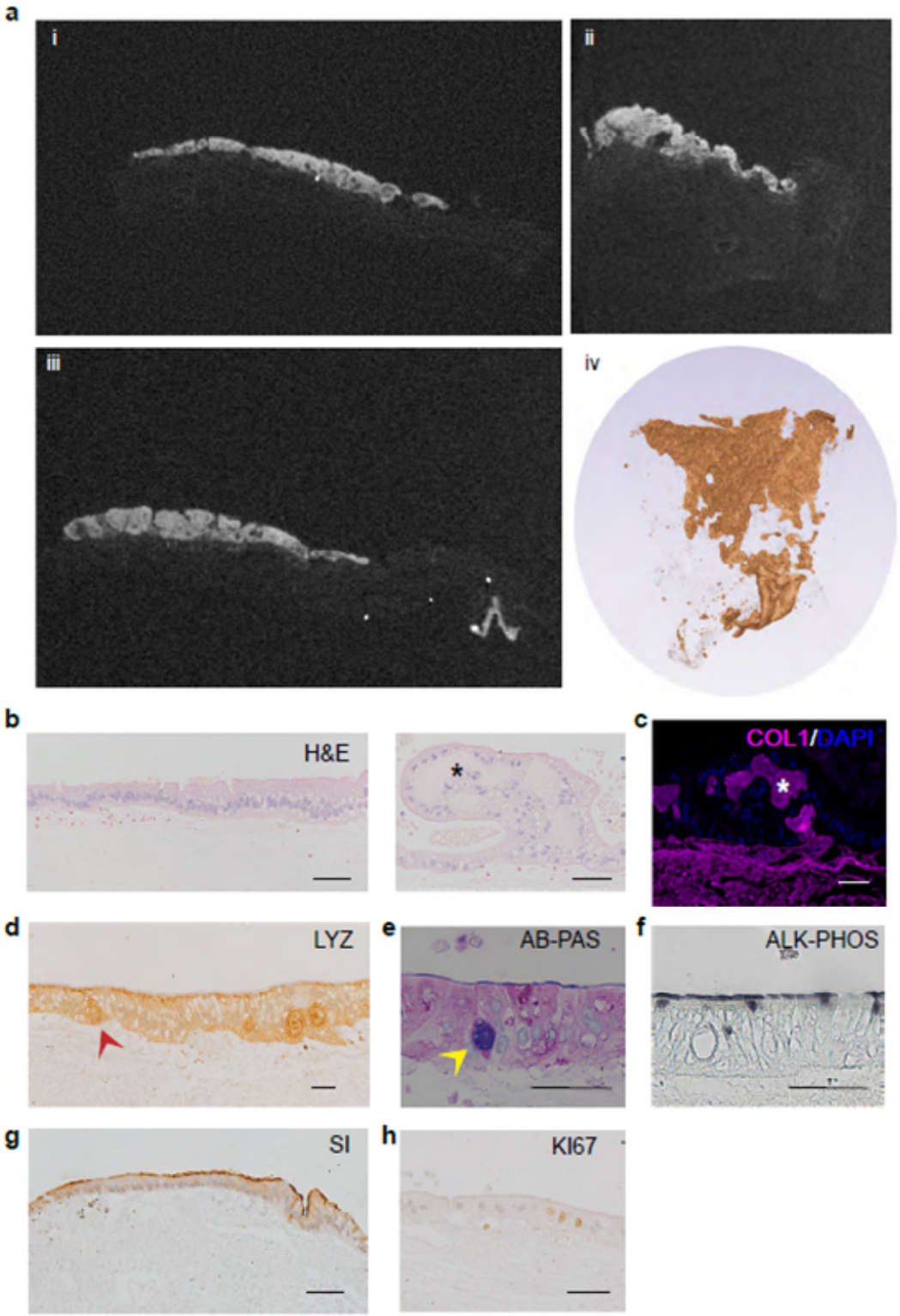

Supplementary Figure 5

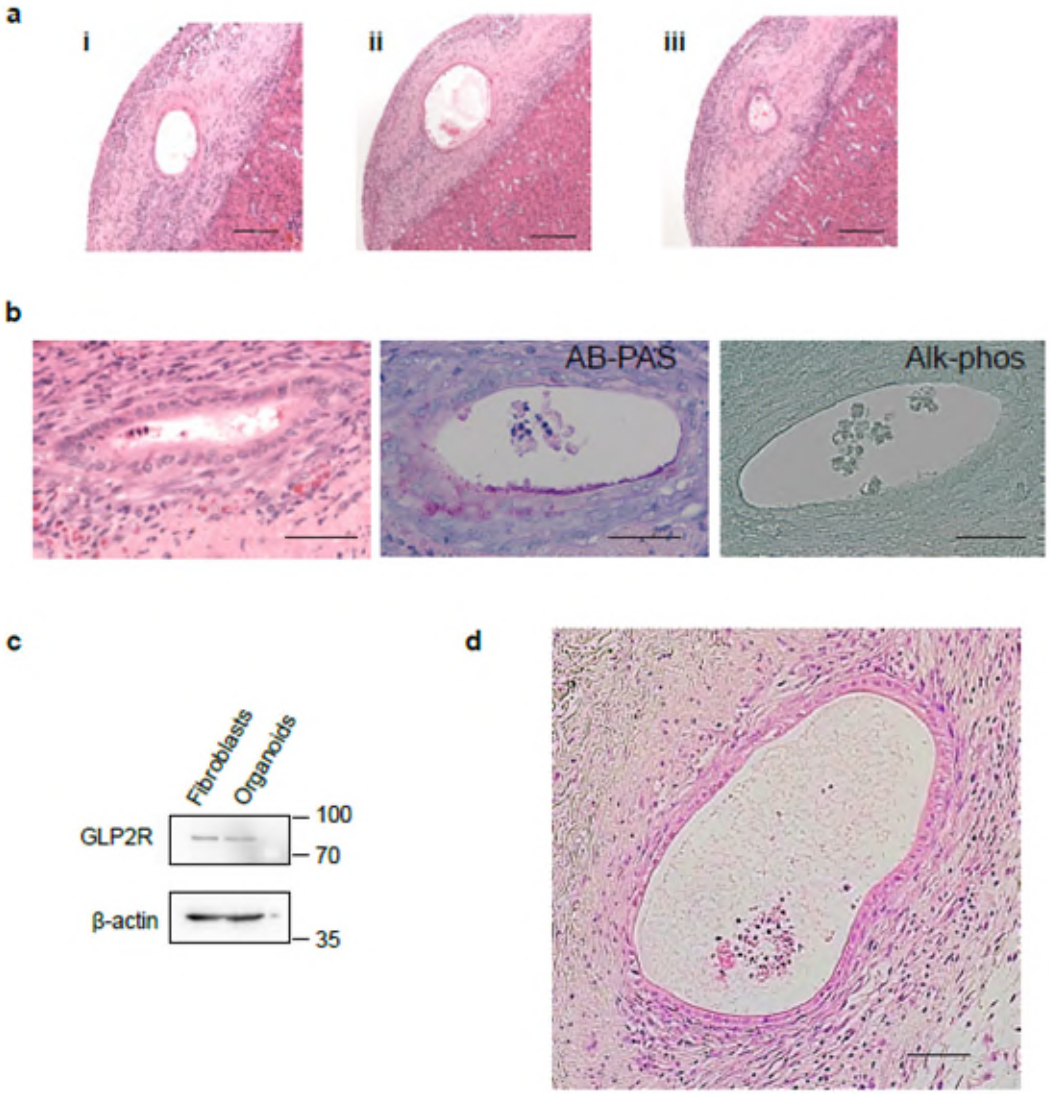

Figure legends

Figure 1 – Generation and characterisation of primary intestinal organoids derived from targeted paediatric patient group
(a) Schematic overview demonstrating the expansion timeline when harvesting intestinal crypts
endoscopically from paediatric patients. (b) Time course cultures of paediatric small intestinal
organoids. (c) First passage expansion of duodenal (i), jejunal (ii) and ileal organoids (iii). Scale bars
represent 200μm. (d) Quantitative RT-qPCR analysis of human duodenal, jejunal and ileal organoids for functional duodenal markers (CYBRD1; SLC40A1), jejunal markers (SI; LCT) and ileal markers (SLC10A2; OSTB). Data represent mean ± s.e.m., the experiment was repeated three times. ***P<0.001, two-way ANOVA. (e) Quantitative RT-qPCR analysis of human jejunal organoids at
37 passages 5, 15 and 25 for jejunal specific markers SI a 900 nd LCT. Data represent mean ± s.e.m. (n=3). ***P < 0.001, two-way ANOVA. (f) Quantitative RT-qPCR analysis of human jejunal organoids treated with GSK3β inhibitor chir99021 (+CHIR), Notch inhibitor (+DAPT). Data represent mean ± s.e.m. (n=3). The experiment was performed three times. *P < 0.5, **P < 0.01, ***P < 0.001, two-way ANOVA. (g) Representative images of EdU incorporation staining of human jejunal organoids in basal culture condition (i) and expansion condition (+CHIR) (ii). Scale bars represent 30μm. (h,i) Representative immunostaining images of human jejunal organoids cultured in expansion conditions (h) or differentiation condition (i) using the indicated antibodies. Scale bars represent 100μm.

Figure 2 - Decellularization of human small intestinal and colon scaffolds
(a,b) Representative images of native human SI (a) and colon (b) before (i) and after decellularization respectively (ii). Scale bars represent 1cm. Representative H&E histological images showing intestinal tissues before (iii) and after decellularization (iv) in both SI (a) and colon (b). Scale bars represent 200μm. Representative images of immunofluorescent staining of intestinal tissues before (iii) and after decellularization (iv) in both SI (a) and colon (b) using the indicated antibodies. Scale bars represent 100μm. (c) Representative images of scanning electron microscopy analysis of the SI (i and iii) and colonic scaffold (ii and iv) highlighting microarchitecture of the mucosa (Mu) submucosa (S) and muscularis (M). Yellow arrow heads indicate intestinal crypts. Red arrow heads indicate villi structure present on the SI scaffold. Scale bars represent 100μm (i and ii) and 10μm (iii and iv).

Figure 3 - Characterization of human decellularized intestinal scaffolds by Raman spectroscopy and mass spectrometry
(a) Average Raman spectra from comparable histological regions of the native tissue (blue lines) and decellularized scaffolds (red lines) of SI (i) and colon (ii) samples. (b) Multivariate curve resolution - alternating lease squares false coloured heat map analysis of Phenylalanine (PHE), Collagen (COL) 38 and Glycosaminoglycans (GAGs) in the human SI and colon sc 925 affolds using Raman microspectroscopy. (c) Principal component analysis score plot used to differentiate the Raman spectra generated from each histologically distinct segments of the small intestine scaffolds (blue) and colonic scaffolds (red). (d) Venn diagrams showing the comparative global total proteins and extracellular proteins detected in the SI and colonic scaffolds by mass spectrometry. Data represents samples from 4 biologically independent patient samples in each group.

Figure 4 - Bioengineering of the human jejunal mucosal graft *in vitro*
(a) Schematic outline of the scaffold seeding strategies under static and dynamic culture using the indicated bioreactor circuit. (b,c) Representative histological images of the jejunal grafts reconstructed using human SI scaffolds (b) or human colonic scaffolds (c) after 14

days of dynamic culture using the indicating staining methods or antibodies. New matrix deposition is shown by newly synthesised collagen (white asterisks). (d) Representative images of electron microscopy analysis of the jejunal constructs showing microvilli (MV) (i and ii); basement membrane with basal lamina (BL) and reticular lamina (RL) at the scaffold (Sc) border (iii); Goblet cell (G) with mucous vesicles indicated by the orange arrow head (iv) and Paneth cell (P) with secretory vesicles indicated by the green arrow head (v). (e) Representative immunofluorescent images of the jejunal grafts seeded on human small intestine scaffolds using the indicated antibodies. All scale bars represent 50μm.

Figure 5 - Functional assessment of the absorptive and digestive capacity of the engineered jejunal graft
(a) Experimental design for the functional analysis of the engineered jejunal grafts. (b) Immunofluorescent staining showing β-AMCA peptide (red) uptake on the jejunal grafts. Phalloidin staining (green) indicates epithelial cell boundaries. High magnification image is shown in (ii). Scale bars represent 30μm. (c) Supernatant of the corresponding jejunal graft culture was collected at days 0, 11 and 25 after organoids seeding for measurement of citrulline concentration. (d) Glucose
39 concentration was measured following a sucrose challenge delivered 950 to each scaffold type at days 4, 11, 18 and 25 of the graft culture (filled lines). Corresponding hashed lines represent baseline glucose production in PBS controls for each scaffold type. All data represents mean ± s.e.m. from 3 independent jejunal grafts constructed using human colon (green line - hColon), human small intestine (red line - hSI) and piglet small intestine (blue line - Piglet) decellularised scaffolds.

Figure 6 - Characterisation of the engineered jejunal graft following *in vivo* transplantation Histological analysis of the Jejunal grafts transplanted under kidney capsule (a-g) or subcutaneously (h-n) for 7 days. (a) Macroscopic image of the kidney harvested after subcapsular implantation of the jejunal grafts (derived from piglet scaffolds); scale bar represents 2mm. (b,c) Histology of the transplanted jejunal graft was analyzed by H&E (b) and human nucleoli staining (c). (d) 3D volume rendered model of the jejunal graft structure transplanted under the kidney capsule. (e-g) Representative immunofluorescent images of the transplanted jejunal grafts using the indicated antibodies. Scale bars represent 50μm. (h) Labelling of the jejunal organoids with luciferase-GFP reporter plasmid for live *in vivo* bioluminescent imaging of the subcutaneous implantation model. Scale bars represent 500μm. (i) Representative histological images of the transplanted jejunal grafts reconstructed using piglet scaffolds using the indicated staining methods or antibodies. Scale bars represent 50μm. (j-n) Histological analysis of the transplanted human jejunal grafts reconstructed using human SI scaffolds using the indicated antibodies. Arrow heads indicate the jejunal epithelium. (l) Electron microscopy analysis identifying mucous granules of goblet cells in the native intestine (i) and jejunal construct (ii,iii). Scale bars represent 20μm. (m,n) Representative immunofluorescent images of the transplanted human jejunal grafts using the indicated antibodies. Scale bars represent 50μm.

Supplementary Figure 1 - Piglet scaffold characterisation
(a) Representative images of H&E and DAPI stainings of the native piglet intestine and following one and two cycles of DET. Scale bars represent 100μm. (b) Quantification of DNA, glycosaminoglycans 40 (GAGs) and Collagen per milligram of wet tissue in native piglet i 975 intestine and following one and two cycles of DET. Data represent mean ± s.e.m using 3 biological replicates. The experiment was repeated 3 times. (c) Representative images of Elastic Van Gieson (EVG) and Alcian blue (AB) stainings confirm preservation of elastin and GAGs respectively following one and two cycles of DET. Representative images of Masson's trichrome (MS) and Picro-sirius red (PS) stainings confirms maintenance of connective tissue and collagens following one and two cycles of DET. Scale bars represent 200μm. (d) Representative images of immunohistochemical staining for Collagen I, Collagen IV, Fibronectin, Laminin indicating the preservation of

these ECM proteins in the scaffold following two cycles of DET. Scale bars represent 100μm.

Supplementary Figure 2 - Characterisation of human decellularized intestinal scaffolds
(a) PC1 loading plot associated with the PC1 vs PC2 scores plot shown in Fig. 3c. The spectral features show the distinct biochemical differences that facilitate the differentiation of the mucosal region of the SI and colon from the remaining intestinal layers (submucosal and muscularis propria). The intensity of the corresponding peaks found within the loadings plot indicate their influence on the separation in the scores plotted along the associated axis. (b,c) Representative
immunohistochemical staining of the native paediatric SI and colon tissue using the indicated antibodies. Scale bars represent 100μm.

Supplementary Figure 3 - Characterisation of primary fibroblasts derived from human intestinal tissues
Representative immunofluorescent images of primary human SI fibroblasts showing fibronectin (a), vimentin (b), fibroblast surface protein marker-1 (c), laminin alpha 5 (d) and alpha-smooth muscle actin (e). Scale bars represent 50μm. 41

Supplementary Figure 4 - Characterisation of the human jejunal graft reconstructed on piglet scaffold
(a) Micro CT virtual slices of jejunal grafts constructed using piglet scaffolds, showing the jejunal epithelial layer (bright white) on the piglet scaffold (i-iii). 3D volume rendering of the epithelium showing nearly full surface coverage (iv). (b) H&E staining of jejunal graft showing regions of columnar epithelial monolayers as well as regions of new matrix deposition (black asterisks). (c) New matrix deposition is indicated by immunofluorescent staining of collagen-1 (magenta) co-stained with DAPI (blue). (d-h) Representative immunohistochemical images of the engineered jejunal grafts using the indicated antibodies. All scale bars represent 50μm.

Supplementary Figure 5 - Histological characterisation of the kidney capsule transplanted graft
(a) Serial sections and H&E staining of the jejunal graft following 7 days transplantation *in vivo* under the kidney capsule. (b) Ring of jejunal graft stains negatively for goblet cells (Alcian Blue - Periodic Acid Schiff) and enterocyte brush border marker (Alkaline Phosphatase). All scale bars represent 50μm. (c) Western blot analysis confirming the expression of the GLP2R in human small intestinal fibroblasts and human jejunal organoids when co-cultured *in vitro*. (d) H&E staining of the jejunal graft seeded on human scaffolds *in vivo* under subcutaneous implantation. Scale bars represent 100μm.